frontiers in Materials

ORIGINAL RESEARCH
published: 26 January 2022
doi: 10.3389/fmats.2021.803054

Hydroxyapatite Growth on Poly (Dimethylsiloxane-Block-ε-Caprolactone)/Tricalcium Phosphate Coatings Obtained by Electrophoretic Deposition

Franco Leonardo Redondo[1,2], *María Carolina Giaroli*[1,2], *Andrés Eduardo Ciolino*[3,4] *and Mario Daniel Ninago*[1,2]*

[1]Universidad Nacional de Cuyo, Facultad de Ciencias Aplicadas a La Industria, San Rafael, Mendoza, Argentina, [2]Consejo Nacional de Investigaciones Científicas y Técnicas (CONICET), Ciudad Autónoma de Buenos Aires, Buenos Aires, Argentina, [3]Planta Piloto de Ingeniería Química, PLAPIQUI (UNS-CONICET), Bahía Blanca, Argentina, [4]Departamento de Ingeniería Química, Universidad Nacional Del Sur (UNS), Bahía Blanca, Argentina

For the first time, composite coatings based on poly(dimethylsiloxane-*block*-ε-caprolactone) copolymer and tricalcium phosphate were obtained on stainless steel plates by using the electrophoretic deposition technique. The effect of different deposition times on the final characteristics of the resulting coatings was also studied. Block copolymers were obtained through a combination of anionic and ring-opening polymerization, with good homogeneity and chemical composition (Đ < 1.3 and w_{PCL} = 0.39). The composites obtained at different electrophoretic deposition times revealed a linear dependence between the deposited weight and time during assays. When immersing in simulated body fluid, a higher amount of residual solids (~ 20 %) were observed by thermogravimetric analysis after 7 days of immersion. Scanning electron microscopy micrographs revealed a porous microstructure over the metallic substrate and the absence of micro-cracks, and X-ray diffraction patterns exhibited diffraction peaks associated with a hydroxyapatite layer. Finally, energy-dispersive X-ray analysis revealed values of the Ca/P ratio between 1.40 and 1.50 in samples, which are closer to the stoichiometric hydroxyapatite values reported in hard tissues. The results obtained in this article confirm the usefulness of poly(dimethylsiloxane-*block*-ε-caprolactone) copolymer and cheaper tricalcium phosphate as precursors of compact and homogenous coatings obtained by electrophoretic deposition, which yields useful substrates for hydroxyapatite growth.

Keywords: block copolymer, tricalcium phosphate, electrophoretic deposition, bioactivity, hydroxyapatite, ring-opening polymerization

OPEN ACCESS

Edited by:
Nafisa Gull,
University of the Punjab, Pakistan

Reviewed by:
Temel Öztürk,
Giresun University, Turkey
Sixun Zheng,
Shanghai Jiao Tong University, China

***Correspondence:**
Mario Daniel Ninago
mninago@fcai.uncu.edu.ar

Specialty section:
This article was submitted to Polymeric and Composite Materials, a section of the journal Frontiers in Materials

Received: *27 October 2021*
Accepted: *27 December 2021*
Published: *26 January 2022*

Citation:
Redondo FL, Giaroli MC, Ciolino AE and Ninago MD (2022) Hydroxyapatite Growth on Poly(Dimethylsiloxane-Block-ε-Caprolactone)/Tricalcium Phosphate Coatings Obtained by Electrophoretic Deposition. Front. Mater. 8:803054. doi: 10.3389/fmats.2021.803054

1 INTRODUCTION

Biocompatible materials play an important role in the area of tissue engineering mainly because they give a new vision of the development materials destined to the repair and regeneration of tissues or the replacement of missing human bones and teeth, among other applications (Qu et al., 2019). One of the main challenges for polymer´s researchers is to develop non-toxic, biodegradable, bioactive, and osteoconductive materials with good mechanical properties at the time of application. For such a purpose, composites formed from two or more materials with excellent properties (polymers,

ceramics, and bioglasses) are widely used in tissue engineering (Yeong et al., 2010; Qu et al., 2019; Bonetti et al., 2020; Ninago et al., 2020; Redondo et al., 2020). Therefore, tissue engineering is a promising area of growing interest in the design and obtaining of polymer-based bioactive materials because of the large number of opportunities that polymeric materials offer.

The use of these materials can be explained according to their ability to be re-absorbed or degraded after a certain time of being implanted without generating toxic products in the receptor organism, and they provide more controllability on physicochemical characteristics such as pore size, porosity, solubility, biocompatibility, enzymatic reactions, and allergic response (Yang et al., 2015; Clavijo et al., 2016; Ghassemi et al., 2018; Quiroga et al., 2018; Ghalayani Esfahani et al., 2019; Taale et al., 2019). In last years, various methodologies capable of developing these new materials have appeared, such as melt mixing (Pishbin et al., 2015), dissolution-leaching (Jordan et al., 2005), and electrophoretic deposition (EPD) technique (El-Ghannam, 2005; Cabanas-Polo and Boccaccini, 2015; Redondo et al., 2020), among others.

The EPD technique is used for the fabrication of coatings because of its simplicity, versatility, and usefulness on substrates with complex geometry (Ghalayani Esfahani et al., 2019; Bonetti et al., 2020; Pereira et al., 2020). EPD is an extremely promising technique for producing organic/inorganic composite scaffolds over several substrates (magnesium, titanium, and stainless steel, among others) to avoid the release of metal ions due to corrosion phenomena (Ghalayani Esfahani et al., 2019; Joy-anne et al., 2019). In addition, a strong union between the material to be implanted and the bone tissue is achieved with this type of methodology (El-Ghannam, 2005; Cabanas-Polo and Boccaccini, 2015). In particular, EPD of soft composites is an attractive technique that can be used to produce uniform coatings with a controlled microstructure, without requiring expensive equipment (Clavijo et al., 2016; Pereira et al., 2020; Redondo et al., 2020). The use of a polymer matrix in biodegradable composites allows obtaining materials with specific geometries and provides a platform for incorporation and release of biomolecules and drugs. These materials can be used in varied applications such as implants in orthopedic surgery, scaffolds, ligament union, sutures, controlled release of drugs, flexible tubes for cardiovascular surgery, and dental repairs, among others (Zhao et al., 2008; Ghasemi-Mobarakeh et al., 2010; Ghalayani Esfahani et al., 2019; Redondo et al., 2020).

Synthetic polymers such as poly(ε-caprolactone) (PCL), poly-lactic acid (PLA), or poly (lactic-co-glycolic) acid (PLGA) are biodegradable and can be used for applications in bone tissue engineering (Boccaccini et al., 2010; Seuss et al., 2016; Pereira et al., 2020). PCL is one of the Food and Drug Administration (FDA)–approved biopolymers and has been extensively used in biomedical applications because of its inherent properties of good mechanical strength, biocompatibility, and biodegradability (Thinakaran et al., 2020). In addition, within the most prominent physicochemical properties of PCL, we can mention its good compatibility with a large variety of polymers (Miola et al., 2015; Joy-anne et al., 2019). Besides, because of being a non-toxic polymer, it is widely used in biomedical applications as long-term implantable devices, scaffolds for tissue growth, drug-delivery systems, and 3D printing or electrospinning devices, among others (Wietor et al., 2011; Liang et al., 2013; Yazdimamaghani et al., 2015; Redondo et al., 2020). PCL or PCL-based copolymers can be obtained by various polymerization techniques such as "click" chemistry, ring-opening polymerization (ROP), or hydrogen-transfer polymerization (Öztürk et al., 2016; Öztürk and Meyvacı, 2017; Savaş et al., 2021). In this sense, ROP is defined as "polymerization in which a cyclic monomer yields a monomeric unit that is either acyclic or contains fewer rings than the cyclic monomer." The technique is widely used for a lot of systems with many monomers, initiators, and catalysts, including lactones and silicones, among others (Öztürk and Meyvacı, 2017).

Silicones, or polysiloxanes, are other biocompatible polymers that are used extensively in the field of biomedicine (Danesin et al., 2012; Redondo et al., 2020). The chemical structure of these polymers has a simple sequence of atoms: polysiloxanes: Si(<)–O–Si(<)–. Usually, substituents at the Si atoms are methyl groups, thus generating the poly(dimethylsiloxane) (PDMS), which is obtained either by polycondensation of $Si(CH_3)_2(Cl)_2$ or by ROP of cyclic monomers, such as hexamethyl (cyclotrisiloxane) (D_3) or octamethyl (cyclotetrasiloxane) (D_4). In addition, PDMS derivatives are widely employed in drug-delivery systems or nanotechnology applications, among others (Nag et al., 2018a; Wolf et al., 2018; Joy-anne, et al., 2019; Luo et al., 2019). PDMS-based organic–inorganic materials have high degrees of flexibility, excellent electrical-insulating properties, and exceptional heat resistance at higher temperatures (Chen et al., 2018; Nag et al., 2018b; Raj et al., 2018; Aoki, 2020). For example, composites from PDMS and ceramic powder allow reducing the thermal stress between the metal substrate and EPD film, while achieving a high thermal conductivity and an enhanced electrical insulation without sintering (Aoki, 2020).

Ceramic materials such as calcium phosphates and silicate glasses are interesting biomaterials due to their bioactivity properties (osteoconduction and osteoinduction) and their ability to form a reactive hydroxyapatite (HA) layer. In recent years, specific compositions of them have been used to obtain hard and soft implants for tissue engineering (Zhou and Lee, 2011; Sartore et al., 2019; Wang et al., 2019; Pereira et al., 2020). The development of bioresorbable and bioactive composites for tissue engineering applications is being investigated worldwide, and many approaches have been published by including combinations of resorbable homopolymers such as PLA, PLGA, and PCL, with HA, tricalcium phosphate ($Ca_3(PO4)_2$, TCP), or bioactive glasses and glass-ceramics in different scaffold architectures (Duruncan and Brown, 2001; Ma et al., 2001; Yang et al., 2005; Ghassemi et al., 2018; Sungsee and Tanrattanakul, 2019). In the most usual approach, HA, TCP, and bioactive glass particles are combined with polymeric biodegradable substrates in order to obtain the desired scaffolds or coatings (Roether et al., 2002; Taale et al., 2019; Mondal et al., 2020; Shah Mohammadi et al., 2020).

HA particles exhibit a chemical composition and crystalline structure similar to that of living bones, and show high

osteoconductivity as well as bioresorbability in biological environments (Maeda et al., 2007; Ramezani et al., 2017). One of the main purposes for employing HA in the synthesis of biodegradable polymeric scaffolds is its ability to modify surface properties in the resulting composites, which are suitable for their use in bone-tissue engineering (Ramezani et al., 2017; Qu et al., 2019; Zhao et al., 2019). The deposition of the HA layer on polymeric materials by using a simulated body-fluid (SBF) solution is often generated by the increase in the supersaturation of inorganic ions in the medium. On the other hand, TCP excels in terms of degradability and bioactivity (two important reasons for its frequent use in clinical applications), and it has attracted much interest since it has been postulated as a precursor of HA formation (Loher et al., 2006). Consequently, it might be reasonable to use TCP as a Ca^{2+} ions–releasing source, by supplying the desired Ca^{2+} ions when immersed in SBF and by promoting HA synthesis (Yu et al., 2018; Dorozhkin, 2010).

In one of the previous work, we reported the capability of block copolymers to induce the precipitation of a HA layer (Redondo et al., 2018; Ninago et al., 2020; Redondo et al., 2020). In this sense, the effect of molecular architecture (linear or branched) of block copolymers and the use of Bioglass® on EPD tests (t = 6 min) was analyzed. It was observed that linear block copolymers promote a better HA deposition when *in vitro* assays were performed. By taking into account these results, in this work, bioactive coatings based on PDMS-*b*-PCL block copolymer and TCP as a mineral filler were employed for HA deposition by using the EPD technique. The emphasis of this work is placed on the combination of these materials for the first time, by obtaining bioactive coatings that promote HA growth. In addition, the effect of EPD time was also studied. It is envisioned that the coatings obtained from this methodology will combine PDMS-*b*-PCL and HA composites in a synergic way, which could be considered as an alternative for scaffolds in bone-tissue engineering (Chen et al., 2019; Qu et al., 2019; Mondal et al., 2020).

2 MATERIALS AND METHODS

Materials

The reagents used for anionic and ROP polymerization were purified by the traditional procedures reported in the literature (Uhrig and Mays, 2005; Redondo et al., 2020). Hexamethyl (cyclotrisiloxane) monomer (D_3, Sigma-Aldrich, 98 %) for anionic polymerization and ε-caprolactone (ε-CL, Sigma-Aldrich, 99 %) for block copolymer synthesis were purified by mixing with the calcium hydride powder (CaH_2, Sigma-Aldrich, 95 %), followed by heating and distilling under vacuum according to conventional procedures. Tetrahydrofuran (THF, Ciccarelli), cyclohexane (Dorwill), and methanol (Química Industrial) were used for the reaction (Agudelo and Pérez, 2016), and stannous octoate was used as a polymerization catalyst (Satti et al., 2017).

For EPD assays, the obtained block copolymers and TCP (CARLO ERBA Reagents) were employed (Boccaccini et al., 2007; Quiroga et al., 2018). Acetone (Sintorgan) was used as a solvent and stainless steel (AISI 316L) plates as metallic substrates. For bioactivity assessments, simulated body fluid (SBF) was prepared according to the suggestions given by Kokubo and Takadama (2006).

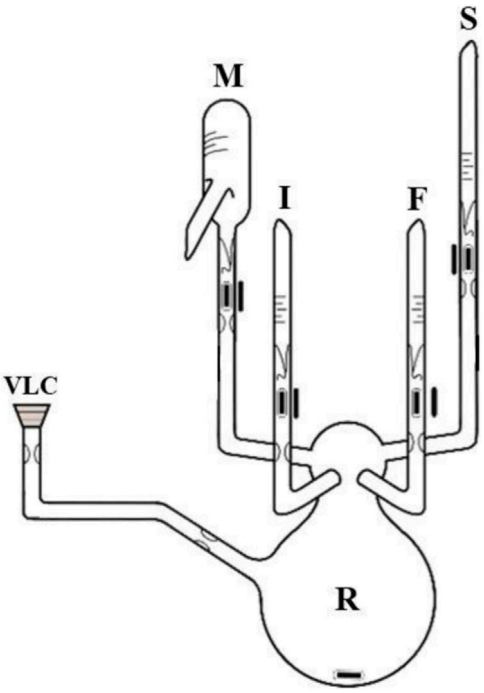

SCHEME 1 | Reactor for PDMS-OH synthesis. References: I: sec-Bu^-Li^+ ampoule; S: THF ampoule; M: D_3 monomer in a cyclohexane ampoule; F: methanol ampoule; R: main reactor; VLC: vacuum line connection.

Synthesis of PDMS-OH Macroinitiator and Linear Block Copolymer

2.1.1 PDMS-OH

The poly(dimethylsiloxane) (PDMS-OH) homopolymer was synthesized by anionic polymerization, employing hand-made polymerization reactors and high-vacuum techniques (**Scheme 1**) (Ninago et al., 2017; Redondo, 2018). In brief, the sealed ampoule of the D_3 monomer (12.5 g, previously dissolved in 40–50 ml of dry cyclohexane) was gently broken and poured into the reactor flask, followed by the addition of the sec-Bu^-Li^+ ampoule (2.9 ml, 0.28 M). The reagents were gently mixed by employing manual movements, and the reaction was left to proceed during ~ 20 h at room temperature. Then, the THF ampoule (10 ml) was broken, and polymerization was left to proceed, at room temperature, during 20 h. The reaction was finished by the addition of the well-degassed methanol ampoule (5 ml), and the resulting PDMS-OH polymer was then precipitated in cold methanol (**Scheme 1**).

2.1.2 PDMS-*B*-PCL Copolymer

The PDMS-*b*-PCL copolymer was synthesized by ROP polymerization of ε-CL monomer, according to the methodology already published by the group (Redondo et al. 2018). Copolymerization was carried out in a glass reactor under

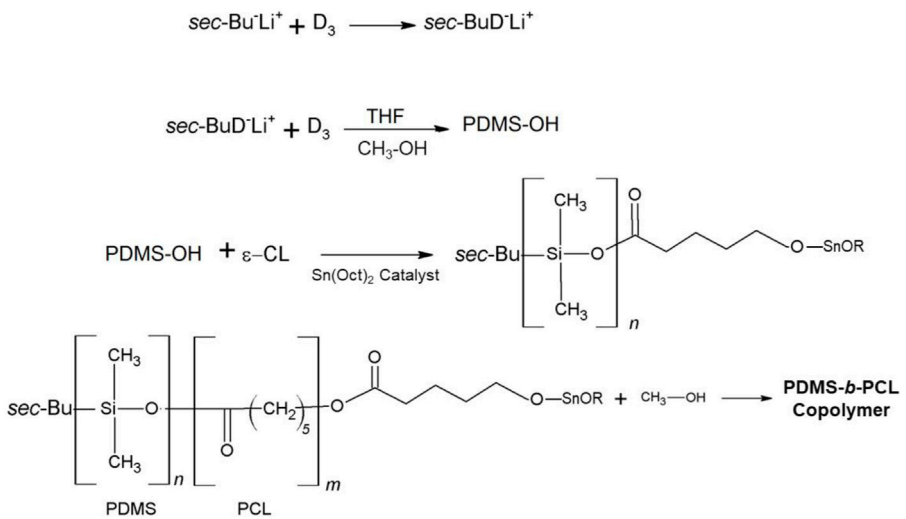

SCHEME 2 | Reaction pathway in the synthesis of PDMS-OH and PDMS-*b*-PCL copolymer.

the nitrogen atmosphere, by employing degassed toluene as a solvent and tin (II) 2-ethylhexanoate ($Sn(Oct)_2$) as a catalyst, at 110°C for 24 h (**Scheme 2**). A catalyst/PDMS-OH ratio of 0.5 was employed (Satti et al., 2017). The obtained copolymers were precipitated, filtered, and stored until their use.

Characterization of the Linear Block Copolymer and TCP Powder

2.1.3 Nuclear Magnetic Resonance (^{1}H-NMR)

The ^{1}H-NMR spectrum of PDMS-*b*-PCL copolymer was performed by using an Avance DPX 400 spectrometer (400 MHz for H and 100 MHz for C) employing $CDCl_3$ as a solvent. From the spectrum, the content of PCL in PDMS-*b*-PCL (the weight fraction of PCL in the copolymer, w_{PCL}) was determined.

2.1.4 Size-Exclusion Chromatography

The molar mass and polydispersity were determined by using an SEC-employing system, a Waters 515 HPLC pump, and a Waters model 410 differential refractometer detector. Toluene and polystyrene were employed as a solvent and standard for calibration, respectively.

2.1.5 Fourier-Transform Infrared Spectroscopy (FTIR-ATR)

Spectra of block copolymer and TCP particles were registered on a Nicolet® iS5 spectrometer, equipped with an attenuated total reflectance accessory (iD7-ATR). Samples were recorded with an accumulation of 16 scans between 3,500–550 cm^{-1} range and a resolution of 4 cm^{-1}.

2.1.6 Differential Scanning Calorimetry

Thermal transitions of PDMS-OH macroinitiator and PDMS-*b*-PCL copolymer were studied on a TA Instruments Calorimeter. Samples (~ 10 mg) were measured under an inert atmosphere of nitrogen, with a flow of 50 ml min^{-1}. First heating was performed from -90–210°C at 10°C min^{-1}. Then, samples were kept at 210°C during 5 min in order to avoid the influence of previous thermal history. After cooling at 10°C min^{-1}, they were heated again from -90–210°C at 10°C min^{-1}. Glass-transition (T_g) and melting temperature (T_m) of PDMS and PCL blocks were determined from this second heating process. With the data obtained, the percentage of crystallinity (% X_c) was obtained by following the equation reported by Yam et al. (1999).

2.1.7 Thermogravimetric Analysis

Thermal stabilities of PDMS-*b*-PCL copolymer and TCP were analyzed by using TGA equipment (Discovery TA Instruments TGA5500 balance). The tests were studied under the nitrogen atmosphere, with a flow of 25 ml min^{-1} and 2°C min^{-1} heating rate, in the 30–700°C range. The percentage of weight loss versus temperature was registered.

2.1.8 Laser Diffraction

Particle-size distribution of TCP was determined by using a Horiba Partica LA-950 Laser Diffraction Particle Size Distribution Analyzer (Kyoto, Japan).

2.1.9 X-Ray Diffraction

The crystal structure identification of TCP was determined by XRD. The patterns were obtained on an Philips PW1710 X-ray diffractometer (Philips, Holland), provided with a tube, a copper anode, and a detector operating at 45 kV and 30 mA within 2θ from 5 to 60°.

2.1.10 Scanning Electron Microscopy

The TCP particles were analyzed by SEM, by using a LEO 40XVP scanning electron microscope, operated at 10 kV. To perform this study, the samples were dispersed over 3M® aluminum

conductive tape by using air flow and coated with gold in an SPI sputter coater. From this analysis, the topographical characteristics of particles were obtained from the secondary electron signal.

Electrophoretic Co-Deposition

Electrophoretic co-deposition assays were performed by following the procedure reported in a previous work (Redondo et al., 2020). For this purpose, a mixture of TCP/copolymer was suspended into a water/acetone solution (10 % v/v) in a [copolymer]:[TCP] ratio equal to 50:50 (wt/wt). It is important to note that prior to the co-EPD deposition procedure, the suspension was stabilized through magnetic stirring and ultrasonic bath for 30 min, by following the procedure previously reported (Redondo et al., 2020). A stainless-steel sample, with rectangular geometry (20 mm × 7 mm x 0.5 mm) was used as a substrate to be coated (working electrode). EPD was carried out by employing an electrophoretic cell connected to an adjustable source (ATTEN model TPR3020S, 220 V/50 Hz). The deposition cell included two parallel stainless-steel foils as a deposition and counter electrodes. The deposition area was fixed at 15 mm × 7 mm, and the distance between electrodes was 10 mm. The deposition conditions for all samples were the following: 20 V by keeping suspension at 56°C and different deposition times: 1, 10, 20, and 30 min. Finally, the samples were removed from suspension and kept in a desiccator, at room temperature.

Characterization of Coatings

2.1.11 Thickness, Deposited Weight, and Thermal Analysis

Coating thicknesses were determined by the use of a digital coating thickness measuring instrument (Digital meter-Microprocessor). Ten values were measured in order to determine the average thickness and standard deviation values. In addition, the deposited weight (W_d) was calculated by employing gravimetric techniques according to **Equation 1**:

$$W_d = \frac{\Delta m}{S_d}, \tag{1}$$

where Δm corresponds to the weight difference between the metallic substrate and the coating, and S_d is the effective deposition area (Redondo et al., 2020).

In addition, the thermal transitions of coatings were studied by employing the aforementioned DSC calorimeter, following the procedure described previously.

In Vitro Assays

Bioactivity tests were carried out by immersion of coatings in SBF during 7 and 28 days at 37°C, replacing SBF solution every 3 days, and by following the protocol already reported by Kokubo and Takadama (2006). FTIR spectra of coatings (before and after being soaked in SBF solution) were obtained by the scratching material employing the aforementioned spectrometer.

Thermal stability of samples after incubation in SBF solution was studied by TGA analysis. Surface appearance of coatings was analyzed by SEM, by using a LEO 40XVP scanning electron microscope, operated at 10 kV. In addition, energy-dispersive X-ray detector (EDX, Model DX-4) with a UTW window was used to quantify the elementary composition of samples. From this analysis, it was possible to visualize the surface of the coatings and the Ca/P ratio. Finally, HA identification was determined by the XRD technique, employing aforementioned equipment.

3 RESULTS AND DISCUSSION

Copolymers and TCP Powder

Figure 1 and **Table 1** summarize the molar mass distribution of PDMS-OH macroinitiator and PDMS-*b*-PCL copolymer. PDMS-OH presents a low dispersity value (Đ = 1.06), which agrees with those obtained by anionic polymerization (almost a symmetric and narrow chromatogram is observed). Besides, PDMS-*b*-PCL shows Đ = 1.36. This value is similar to the values reported in the scientific literature for the synthesis of homopolymers and copolymers based of ε-CL using ROP (Duruncan and Brown, 2001; Ma et al., 2001; Redondo, 2018; Wang et al., 2019). In addition, a clear shift of the PDMS-*b*-PCL chromatogram is also observed in **Figure 1**. This fact constitutes clear evidence of the increase in molar mass due to the incorporation of the PCL block in the resulting copolymer. The PCL content in PDMS-*b*-PCL copolymer was determined by ^{1}H-NMR as w_{PCL} = 0.39 (Zhou and Lee, 2011; Sultana, 2018).

Figure 2 shows the FTIR-ATR spectra of the TCP precursor, PDMS-OH macroinitiator, and PDMS-*b*-PCL copolymer. PDMS-OH macroinitiator exhibits the typical absorption bands detected at 2,963 cm^{-1} (associated with C–H vibration bonds attached to Si atoms) (Liang and Ruckenstein, 1996; Wu et al., 2006; Redondo, 2018); 1,261 cm^{-1} (associated with out-of-phase vibrations of -Si(CH$_3$)$_2$- and O–Si–O groups) (Agudelo and Pérez, 2016); and 1,094, 1,024, and 801 cm^{-1} (bands associated with the vibration of the Si–O–Si and C–Si–C bonds, respectively) (Agudelo and Pérez, 2016; Ninago et al., 2017; Redondo, 2018). Regarding to PDMS-*b*-PCL copolymer, absorption bands associated to the PCL block are observed at 2,960 and 2,865 cm^{-1} (vibration bands from methylene, -CH$_2$, groups) and 1,724 cm^{-1} (a pronounced signal attributed to the stretching vibrations from carbonyl groups, >C=O) (Redondo, 2018). In addition, the corresponding absorption bands associated to the PDMS block are also observed at 1,260, 1,091, 1,032, and 801 cm^{-1}. On the other hand, the TCP spectrum shows absorption bands at 1,088, 561, and 600 cm^{-1} (bands associated with bending out-of-plane of the PO$_4^{3-}$ group); 1,026 and 962 cm^{-1} (bands associated with the asymmetric vibration of the PO$_4^{3-}$ group); and typical absorption bands of TCP (Peña and Vallet- Regı, 2003; Reid et al., 2006; Mohandes and Salavati-Niasari, 2014a; Park et al., 2014).

Figure 3 shows X-ray diffraction patterns of TCP. Twelve peaks associated to the structure of TCP are detected at 2Θ ~ 24.8°, 25.8°, 28.1°, 29.0°, 31.8°, 32.8°, 34.1°, 39.8°, 46.7°, 48.1°, 49.5°, and 53.1° (Cordero-Arias et al., 2015). The most prominent peaks in the diffractogram are the following: 2Θ ~ 25.8°, 31.8°, 39.8°, 46.7°, and 53.1°, which correspond to the planes (002), (211),

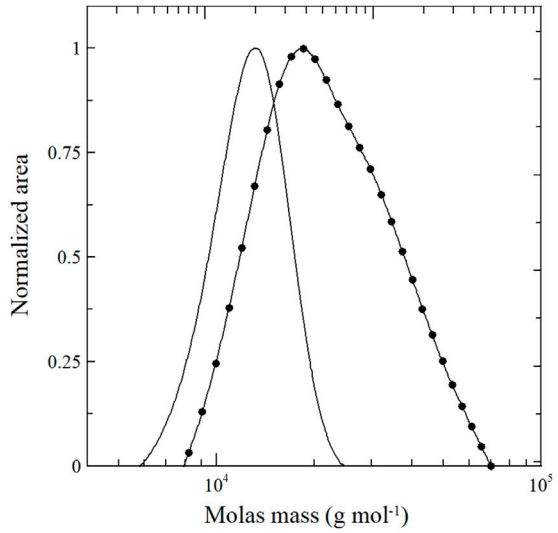

FIGURE 1 | SEC chromatograms: (-) PDMS-OH macroinitiator and (●) PDMS-*b*-PCL copolymer.

(221), (222) y, and (004), respectively (Lala et al., 2016; Aguiar et al., 2018).

The distribution of the particle size from the TCP powder is shown in **Figure 4A**. From LD analysis, an average size of 12.1 μm in a unimodal distribution with a smaller population shoulder (with an average size of 2.9 μm) was determined. The SEM micrograph of TCP shows irregular particles with conglomerates of asymmetric morphology (**Figure 4B**), in accordance with the literature reported by Ginebra et al. (2004) and Nagase et al. (1989).

The thermal characterization of synthesized polymers is shown in **Table 1** and **Figure 5**. Regarding to DSC measurements, PDMS-OH macroinitiator presents only a thermal transition (T_{mPDMS}) in the range of temperature analyzed. Besides, three thermal transitions are detected in PDMS-*b*-PCL copolymer: T_{gPCL} and T_{mPCL} of the PCL block and T_{mPDMS} of the PDMS semi-crystalline phase (Redondo et al., 2018). Besides, % crystallinity (X_c) was obtained by taking into account the PCL content and ΔH_{ref} = 136.1 J g^{-1} (Yam et al., 1999). The value of X_c is reduced in PDMS-*b*-PCL copolymer (26.3 %) when comparing to reference PCL homopolymer (44.7 %) due to the coupling of the PDMS block. Moreover, two thermal transitions were detected in PCL homopolymer: T_{gPCL} and T_{mPCL}.

On the other hand, the thermal degradation initiation temperature ($T_{0.05}$, for 5% mass loss) was calculated from TGA curves (not shown). PDMS-OH macroinitiator shows a $T_{0.05}$ value at ~ 304°C (Ninago et al., 2013; Ramezani et al., 2017; Redondo, 2018). PCL homopolymer shows a $T_{0.05}$ value at 341.5°C, becoming more noticeable after approximately 400°C (the thermal degradation event which corresponds to polyester chain decomposition) (Cai et al., 2014; Ninago et al., 2015; Redondo, 2018). On the other hand, the following degradation events in the copolymer were detected at 193°C (associated to the rupture of polyester chains through the ester pyrolysis reaction generating H_2O, CO_2, and 5-hexenoic acid); at 289°C (associated to the PCL block decomposition); and at 366°C (associated to the PDMS block degradation) (Persenaire et al., 2001; Ninago et al., 2013; Redondo et al., 2018). Regarding to TCP, no decomposition event was observed in the studied range.

Characterization of Coatings

Figure 6 shows thickness and deposited weight values for the coatings obtained at different test times: 1, 10, 20, and 30 min. A linear dependence between deposited weight and time was observed (an R^2 value of 0.98). In addition, an increase in the thickness is also observed for higher EDP times at constant deposition voltage. In accordance, higher thickness and weight values are found at 30 min of EPD assay. In order to obtain thicker coatings, it is convenient to extend the EPD time. In this sense, Bartmanski et al. (2019) and Wang et al. (2002) reported the same behavior in EPD tests obtaining a nanohydroxyapatite coating. These authors stressed that the prolongation of EPD time did not cause any adverse effects on the coating structure and resulted in a significantly higher thickness of the coatings. On the other hand, **Figure 5** includes the thermal transitions of the coatings obtained. In this sense, the glass transition and melting point of the PCL block were detected at −64.0°C and 57.5°C, respectively. Besides, the thermal transition of the PDMS block was also detected at −45.2°C. In addition, a significant reduction in the X_c value for PCL is observed: 3.3 % due to the incorporation of TCP particles interfere in the ordering of the PCL chains during the crystallization process. This phenomenon encourages the decreasing of the X_c value. Chen et al. (2014) reported a similar behavior during the study of PCL composites reinforced with bioactive particles.

TABLE 1 | Thermal characterization of synthesized polymers.

Sample	M_n [a] (g mol^{-1})	Đ [a]	w_{PCL} [b]	T_{gPCL} [c] (°C)	T_{mPDMS} [c] (°C)	T_{mPCL} [c] (°C)	X_c [c] (°C)	$T_{0.05}$ [d] (°C)
PDMS-OH	12,300	1.06	--	--	-44.9	--	n/a	304.0
PCL	26,000	1.60	1.00	⁻66.0	--	55.9	44.7	341.5
PDMS-*b*-PCL	21,300	1.36	0.39	⁻59.1	⁻42.4	50.4	26.3	205.1

[a]*Number average molar mass (M_n) and dispersity (Đ) determined by SEC and ^{1}H-NMR.*
[b]*Weight fraction of PCL in copolymers (w_{PCL}) determined by ^{1}H-NMR.*
[c]*Glass-transition temperature (T_g), melting temperature (T_m), and degree of crystallinity (X_c) determined by DSC.*
[d]*5 % thermal degradation temperature ($T_{0.05}$) determined by TGA.*

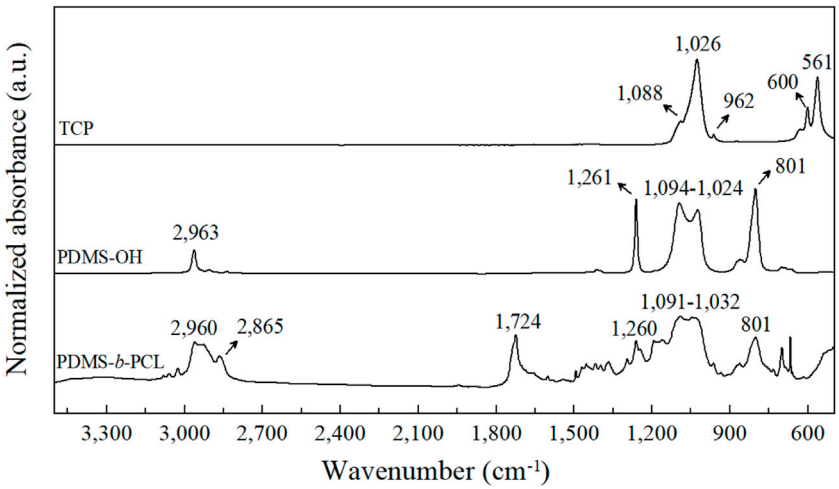

FIGURE 2 | Normalized FTIR-ATR spectra of TCP particles, PDMS-OH macroinitiator, and PDMS-*b*-PCL copolymer (spectra were shifted from the *y*-axis in order to show differences).

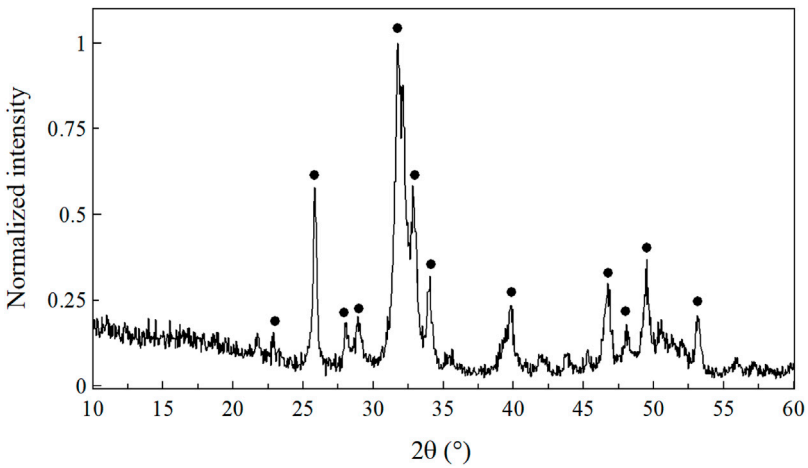

FIGURE 3 | XRD spectrum of TCP particles.

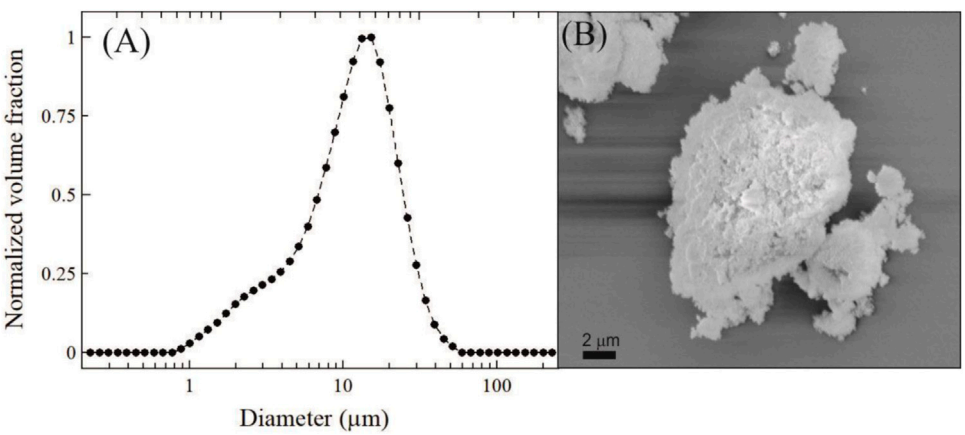

FIGURE 4 | (A) Particle size distribution of TCP by LD and **(B)** SEM micrograph of TCP particles.

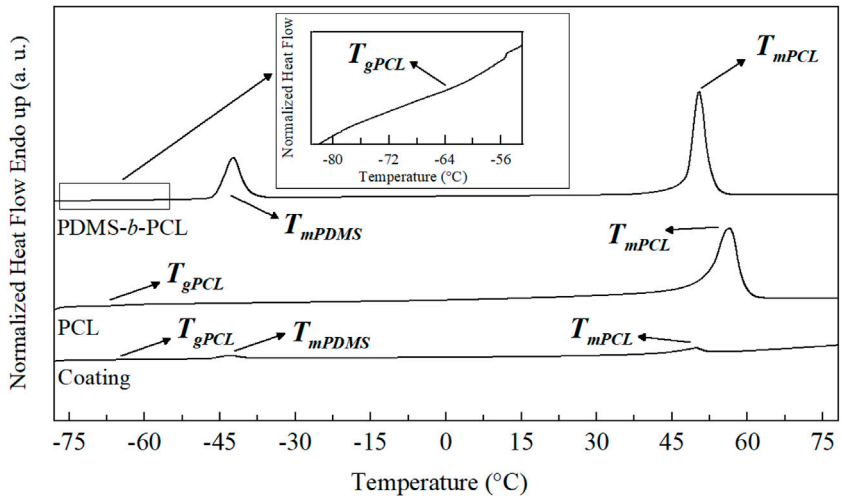

FIGURE 5 | Thermal transitions of PDMS-*b*-PCL copolymer, PCL homopolymer, and coating (before soaking in SBF solution) by DSC.

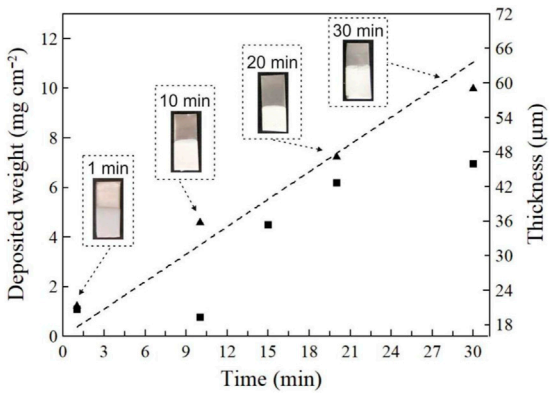

FIGURE 6 | (■) Thickness and (▲) deposited weight of coatings obtained by EPD procedures.

In Vitro Assays

In vitro assays were performed by soaking in SBF solution for 7 and 28 days. For these tests, the sample with higher thickness and weight values was selected (t = 30 min for EPD co-deposition).

Figure 7 shows the normalized FTIR-ATR spectra of the coating before and after immersion in SBF solution for 7 and 28 days, respectively. PCL and PDMS absorption bands are distinguishable in all samples as well as the absorption bands at 1,024 and 600 cm^{-1} (bands associated with the asymmetric vibration and bending out-of-plane of the PO_4^{3-} group, respectively [Peña and Vallet- Regı, 2003; Reid et al., 2006; Mohandes and Salavati-Niasari, 2014a; Park et al., 2014]) attributed to the TCP filler.

After immersion in SBF solution, new vibration bands were detected at 3,183 cm^{-1} (stretching vibration attributed to the crystal water and surface-adsorbed water molecules), 1,629 cm^{-1} (vibrations of the –COOH group), and 1,552 cm^{-1} (vibration of the CO_3^{2-} group). These results are in good agreement with those described by Mohandes and Salavati-Niasari (2014b). In addition, this fact could be explained considering the formation of carboxylic ethers in the coatings and their interaction with a new-formed HA phase on the surface (Chen et al., 2014; Mohandes and Salavati-Niasari, 2014b).

Figure 8 shows X-ray diffraction patterns of coatings after being soaked in SBF solution during 7 and 28 days. XRD patterns of coatings exhibit diffraction peaks associated to the HA phase (Chen et al., 2014). The existence of characteristic diffraction peaks associated with the HA phase are detected at 2Θ values of 26.0°, 31.9°, 33.0°, 34.1°, 39.9°, 46.8°, 49.6°, and 53.3°, corresponding to the diffraction planes (002), (211), (300), (202), (310), (222), (213), and (004), respectively (Mohandes and Salavati-Niasari, 2014a; Mohandes and Salavati-Niasari, 2014b; Miola et al., 2015; Lala et al., 2016; Redondo et al., 2020). This fact confirms the effectiveness of the mineralization process. A similar behavior was observed in a previous work, where composite coatings were obtained by employing the same copolymer and Bioglass® as an inorganic filler. The presence of HA was also detected as an acute and intense signal that appeared at 2Θ ~ 31.8° and other characteristic diffraction peaks at 2Θ ~ 25.9°, 29°, 39°, and 46.7° (Redondo et al., 2020).

In a similar analysis, Dorozhkin (2010) and Suchanek and Yoshimura (1998) stressed that chemical changes can occur in bioceramic materials when they are exposed to *in vitro* conditions. Therefore, in an acidic medium, it was found that TCP particles can be partially dissolved by causing the liberation of Ca^{2+} and PO_4^{3-} ions to the solution. Consequently, the increase of ions leads to the supersaturation of the biologic fluid by promoting the precipitation of biological HA nanocrystals. In this context, Roether et al., (2002) reported that HA is formed on PLA/Bioglass composite materials after 7 days of immersion in SBF. Zhang et al., (2004) also reported that after 7 days of immersion in SBF, PLA/Bioglass composite

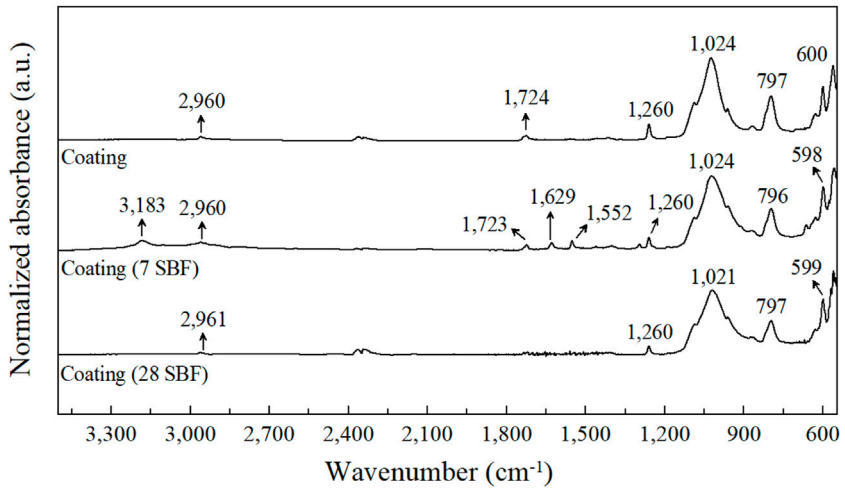

FIGURE 7 | Normalized FTIR-ATR spectra of coatings before and after soaking in SBF solution.

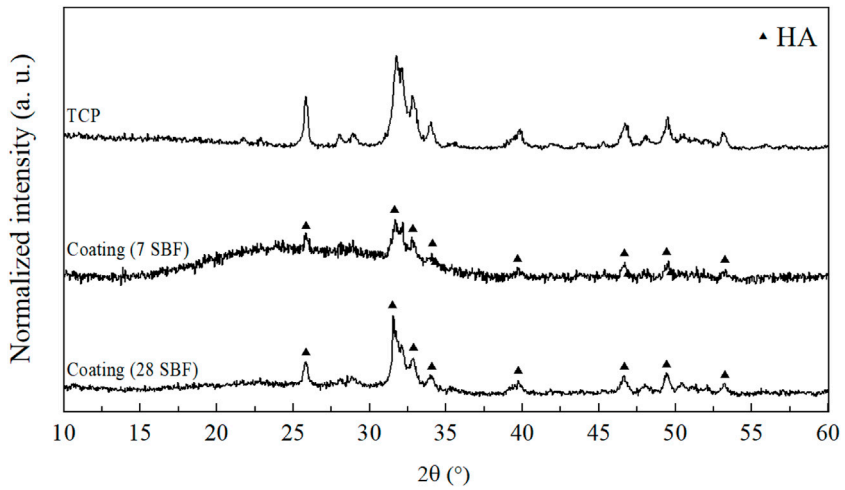

FIGURE 8 | XRD spectra of coatings after immersion in SBF solution.

materials fabricated by using thermally induced phase separation (TIPS) developed HA on their surfaces. In addition, the absence of stainless-steel substrate peaks confirms the successful co-deposition methodology employed. According to the obtained results, TCP/PDMS-*b*-PCL coatings evidenced the ability to form a HA layer onto the composite substrate (Zhang et al., 2004; Maeda et al., 2007).

Thermogravimetric tests before and after *in vitro* assessment are shown in **Figure 9**. Weight loss events in coatings before being soaked in SBF solution are undoubtedly attributed to degradation processes of polymeric chains of PDMS and PCL since TCP particles present thermal stability without degradation events at TGA test temperatures.

The coatings exhibit a slight reduction in $T_{0.05}$ temperatures (239.2°C) when comparing to their respective polymers. The TGA curve of the coating shows a weight loss event associated to the rupture of the PCL block at 236°C, while the PDMS block degradation is evidenced at 368°C (see the two peaks in the first derivative dW/dT). The TGA analysis showed the individual decomposition temperatures of the polymeric blocks that constitute the copolymer. Öztürk et al., (2013) reported the same behavior for the thermal analysis of triarm block copolymers of poly(styrene-*block*-β-butyrolactone) (PS-*b*-PBL). Regarding to the coating after being soaked in SBF solution, only an event of degradation was observed. The decomposition started at 300°C, and it is completed at 400°C, by reaching ~ 89 % weight loss. The first derivative dW/dT curve shows a single peak at 365°C.

When comparing, the weight loss percentage for the coating before immersion in SBF solution is lower than that of the coating

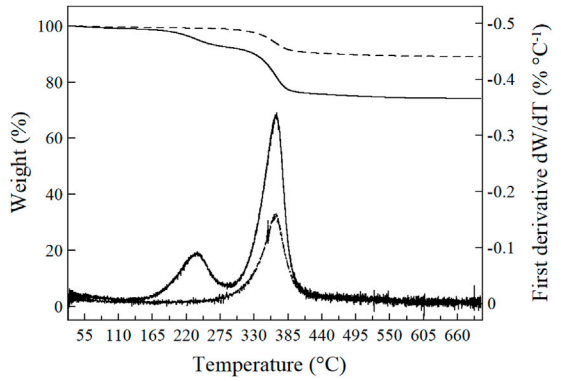

FIGURE 9 | TGA and first derivative dW/dT curves of the coating before (-) and after (--) immersion in SBF solution during 7 days.

after immersion in SBF solution. These results could be indicating that the coating after immersion in SBF solution has a higher content of the HA precipitate itself. This behavior could be attributed to a better transformation of TCP into HA by a dissolution–precipitation mechanism, which produces a new inorganic phase (Suchanek and Yoshimura, 1998; Somrani et al., 2003). Besides, it was possible to calculate the value of the experimental [Polymer]:[TCP]$_e$ wt/wt ratio. The samples tested show a higher TCP value when compared to the theoretical value (50:50 wt/wt). That is to say, coatings before and after immersion in SBF solution presented [Polymer]:[TCP]$_e$ ratios equal to 26:74 (wt/wt) and 11:89 (wt/wt), respectively. In this sense, the macromolecular structure in blocks encourages a higher TCP deposition due to higher values was obtained after soaking in SBF solution.

Figure 10 shows the SEM images of coatings after immersion in SBF solution during 7 days (**Figure 10A**) and 28 days (**Figure 10B**). In addition, EDX patterns were also included in the figure in order to analyze the elementary composition of coatings as well as the Ca/P ratio. A microporous structure is observed in the SEM micrographs, with a thin continuous layer without superficial fractures that covered the metallic substrate. Besides, a more compact and uniform coating (surface covered) is obtained for longer immersion times. **Figure 10B** reveals a more compact and smoother surface, whereas **Figure 10A** exhibits the presence of aggregates and a porous structure. Moreover, TCP particles are evenly distributed within the polymer matrix, obtaining a good mix between materials. Fauré et al., (2012) reported a similar behavior of bioactive particles during the EPD methodology: the particles that settle induce the incorporation of more particles on the coating, thus achieving surfaces with the interconnected macroporous and microporous structure.

Finally, EDX analysis revealed a value of the Ca/P ratio between 1.40 and 1.50 for both immersion times (7 and 28 days), by exhibiting values closer to those reported in the literature (Raynaud et al., 2002; Yu et al., 2018). In this sense,

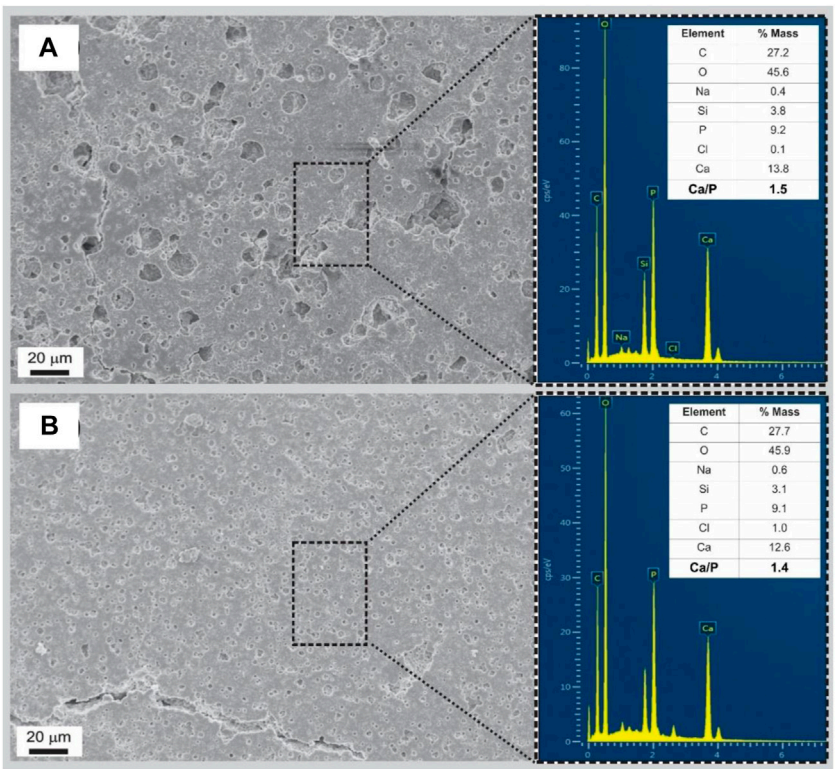

FIGURE 10 | SEM micrographs (1,000x) and EDX spectra of coatings after immersion in SBF solution during **(A)** 7 days and **(B)** 28 days.

Raynaud et al., (2002) and Yu et al., (2018) reported the same behavior by using powders of apatite calcium phosphate with the Ca/P ratio ranging from 1.50 to 1.67. These authors stressed that HA growing could be attributed to the higher diffusion rate of calcium species relative to that of phosphate anions inside the polymeric matrix, which leads to a higher release of calcium from the surface. Altogether, this induces a rapid formation of a thin HA layer owing to the large surface area over which it is distributed and significantly decreases when the PO_4^{3-} content in the solution approaches zero (Yu et al., 2018).

According to Ramezani et al., (2017), the rapid exchange of Ca^{2+} and Mg^{2+} ions with H^+ or H_3O^+ from SBF solution increases the hydroxyl concentration of the solution. This change leads to the superficial modification of the coating, which causes HA nucleation. Then, the migration of PO_4^{3-}, Ca^{2+}, and OH^- ions from the surrounding fluid to the surface of the coating accelerates the nucleation and precipitation of an HA layer (Ramezani et al., 2017; Yu et al., 2018). In this sense, it is plausible that the synergistic effects of co-EPD time + TCP/PDMS-*b*-PCL promote a coating surface that induces the further HA growth.

4 CONCLUSION

Poly(dimethylsiloxane-*block*-ε-caprolactone) copolymer was obtained by a combination of anionic and ring-opening polymerization. The resulting block copolymer showed a good compatibility with the tricalcium phosphate powder to obtain compact and potentially bioactive coatings by electrophoretic deposition. A linear dependence of deposited weight and thickness was observed for electrodeposition time. After *in vitro* assays in SBF solution, new absorption bands and new patterns assigned to tricalcium phosphate were detected by FTIR-ATR and XRD analysis, while SEM-EDX analysis revealed similar Ca/P ratio values those reported for natural bone tissues. According to these results, the coatings obtained in this work evidence an enhanced capacity to induce the precipitation of tricalcium phosphate and suggest the chemical transformation of tricalcium phosphate into HA through a dissolution–precipitation mechanism.

DATA AVAILABILITY STATEMENT

The raw data supporting the conclusions of this article will be made available by the authors, without undue reservation.

AUTHOR CONTRIBUTIONS

FR, MG, AC, and MN conceived the study, performed the experimental analysis as well as the interpretation of data, and drafted the manuscript. In addition, all authors read and approved the final manuscript.

FUNDING

This work was supported by the Fondo para la Investigación Científica y Tecnológica (FONCyT, Argentina) under grant (PICT-2016-0181) and Universidad Nacional de Cuyo (UNCuyo, Argentina) under grant (SIIP 06/L030-B; SeCTyP PROJOVIN).

ACKNOWLEDGMENTS

The authors wish to thank the Consejo Nacional de Investigaciones Científicas y Técnicas (CONICET, Argentina).

REFERENCES

Agudelo, N. A., and Pérez, L. D. (2016). Synthesis and Characterization of Polydimethylsiloxane End-Modified Polystyrene from Poly(Styrene - Co -Vinyltriethoxysilane) Copolymers. *Mat. Res.* 19 (2), 459–465. doi:10.1590/1980-5373-MR-2015-0599

Aguiar, H., Chiussi, S., López-Álvarez, M., González, P., and Serra, J. (2018). Structural Characterization of Bioceramics and Mineralized Tissues Based on Raman and XRD Techniques. *Ceramics Int.* 44 (1), 495–504. doi:10.1016/j.ceramint.2017.09.203

Aoki, Y. (2020). Superhydrophobic Coating Fabricated by Electrophoretic Deposition Using Polydimethylsiloxane-Based Organic-Inorganic Hybrid Materials and Ceramic Powders. *Mol. Cryst. Liquid Cryst.* 704 (1), 10–16. doi:10.1080/15421406.2020.1741795

Bartmanski, M., Zielinski, A., Jazdzewska, M., Głodowska, J., and Kalka, P. (2019). Effects of Electrophoretic Deposition Times and Nanotubular Oxide Surfaces on Properties of the Nanohydroxyapatite/nanocopper Coating on the Ti13Zr13Nb alloy. *Ceram. Int.* 45 (16), 20002–20010. doi:10.1016/j.ceramint.2019.06.258

Boccaccini, A. R., Chen, Q., Lefebvre, L., Gremillard, L., and Chevalier, J. (2007). Sintering, Crystallisation and Biodegradation Behaviour of Bioglass-Derived Glass-Ceramics. *Faraday Discuss.* 136, 27–44. doi:10.1039/B616539G

Boccaccini, A. R., Keim, S., Ma, R., Li, Y., and Zhitomirsky, I. (2010). Electrophoretic Deposition of Biomaterials. *J. R. Soc. Interf.* 7 (Suppl. l_5), S581–S613. doi:10.1098/rsif.2010.0156.focus

Bonetti, L., Altomare, L., Bono, N., Panno, E., Campiglio, C. E., Draghi, L., et al. (2020). Electrophoretic Processing of Chitosan Based Composite Scaffolds with Nb-Doped Bioactive Glass for Bone Tissue Regeneration. *J. Mater. Sci. Mater. Med.* 31 (5), 1–12. doi:10.1007/s10856-020-06378-6

Cabanas-Polo, S., and Boccaccini, A. R. (2015). Understanding Bioactive Glass Powder Suspensions for Electrophoretic Deposition of Bioactive Glass-Polymer Coatings. *J. Electrochem. Soc.* 162 (11), D3077–D3083. doi:10.1149/2.0211511jes

Cai, J., Xiong, Z., Zhou, M., Tan, J., Zeng, F., MeihuMa, S., et al. (2014). Thermal Properties and Crystallization Behavior of Thermoplastic Starch/Poly(ε-Caprolactone) Composites. *Carbohydr. Polym.* 102, 746–754. doi:10.1016/j.carbpol.2013.10.095

Chen, Q., Cabanas-Polo, S., Goudouri, O.-M., and Boccaccini, A. R. (2014). Electrophoretic Co-deposition of Polyvinyl Alcohol (PVA) Reinforced Alginate-Bioglass Composite Coating on Stainless Steel: Mechanical Properties and *In-Vitro* Bioactivity Assessment. *Mater. Sci. Eng. C* 40, 55–64. doi:10.1016/j.msec.2014.03.019

Chen, J., Zheng, J., Gao, Q., Zhang, J., Zhang, J., Omisore, O., et al. (2018). Polydimethylsiloxane (PDMS)-based Flexible Resistive Strain Sensors for Wearable Applications. *Appl. Sci.* 8 (3), 345. doi:10.3390/app8030345

Chen, C.-C., Lee, S.-Y., Teng, N.-C., Hu, H.-T., Huang, P.-C., and Yang, J.-C. (2019). *In Vitro* and *In Vivo* Studies of Hydrophilic Electrospun PLA95/β-TCP Membranes for Guided Tissue Regeneration (GTR) Applications. *Nanomaterials* 9 (4), 599. doi:10.3390/nano9040599

Clavijo, S., Membrives, F., Quiroga, G., Boccaccini, A. R., and Santillán, M. J. (2016). Electrophoretic Deposition of Chitosan/Bioglass® and Chitosan/Bioglass®/TiO2 Composite Coatings for Bioimplants. *Ceram. Int.* 42 (12), 14206–14213. doi:10.1016/j.ceramint.2016.05.178

Cordero-Arias, L., Cabanas-Polo, S., Goudouri, O. M., Misra, S. K., Gilabert, J., Valsami-Jones, E., et al. (2015). Electrophoretic Deposition of ZnO/alginate and ZnO-Bioactive Glass/alginate Composite Coatings for Antimicrobial Applications. *Mater. Sci. Eng. C* 55, 137–144. doi:10.1016/j.msec.2015.05.034

Danesin, R., Brun, P., Roso, M., Delaunay, F., Samouillan, V., Brunelli, K., et al. (2012). Self-assembling Peptide-Enriched Electrospun Polycaprolactone Scaffolds Promote the H-Osteoblast Adhesion and Modulate Differentiation-Associated Gene Expression. *Bone* 51 (5), 851–859. doi:10.1016/j.bone.2012.08.119

Dorozhkin, S. V. (2010). Bioceramics of Calcium Orthophosphates. *Biomaterials* 31 (7), 1465–1485. doi:10.1016/j.biomaterials.2009.11.050

Duruncan, C., and Brown, P. W. (2001). Biodegradable Hydroxyapatite–Polymer Composites. *Adv. Eng. Mater.* 3 (4), 227–231. doi:10.1002/1527-2648(200104)3:4<227::aid-adem227>3.0.co;2-1

El-Ghannam, A. (2005). Bone Reconstruction: from Bioceramics to Tissue Engineering. *Expert Rev. Med. Devices* 2 (1), 87–101. doi:10.1586/17434440.2.1.87

Fauré, J., Drevet, R., Potiron, S., Gordin, D. M., Oudadesse, H., Gloriant, T., et al. (2012). "Electrophoretic Deposition of Bioactive Glass Coatings on Ti12Mo5Ta alloy," in *Key Engineering Materials* (Switzerland: Trans Tech Publications Ltd), 135–140.

Ghalayani Esfahani, A., Soleimanzade, M., Campiglio, C. E., Federici, A., Altomare, L., Draghi, L., et al. (2019). Hierarchical Microchannel Architecture in Chitosan/bioactive Glass Scaffolds via Electrophoretic Deposition Positive-replica. *J. Biomed. Mater. Res.* 107 (7), 1455–1465. doi:10.1002/jbm.a.36660

Ghasemi-Mobarakeh, L., Prabhakaran, M. P., Morshed, M., Nasr-Esfahani, M. H., and Ramakrishna, S. (2010). Bio-functionalized PCL Nanofibrous Scaffolds for Nerve Tissue Engineering. *Mater. Sci. Eng. C* 30 (8), 1129–1136. doi:10.1016/j.msec.2010.06.004

Ghassemi, T., Shahroodi, A., Ebrahimzadeh, M. H., Mousavian, A., Movaffagh, J., and Moradi, A. (2018). Current Concepts in Scaffolding for Bone Tissue Engineering. *Arch. Bone Jt. Surg.* 6 (2), 90–99. doi:10.22038/abjs.2018.26340.1713

Ginebra, M. P., Driessens, F. C. M., and Planell, J. A. (2004). Effect of the Particle Size on the Micro and Nanostructural Features of a Calcium Phosphate Cement: A Kinetic Analysis. *Biomaterials* 25 (17), 3453–3462. doi:10.1016/j.biomaterials.2003.10.049

Jordan, J., Jacob, K. I., Tannenbaum, R., Sharaf, M. A., and Jasiuk, I. (2005). Experimental Trends in Polymer Nanocomposites-A Review. *Mater. Sci. Eng. A* 393 (1-2), 1–11. doi:10.1016/j.msea.2004.09.044

Oliver, J.-a. N., Su, Y., Lu, X., Kuo, P.-H., Du, J., and Zhu, D. (2019). Bioactive Glass Coatings on Metallic Implants for Biomedical Applications. *Bioactive Mater.* 4, 261–270. doi:10.1016/j.bioactmat.2019.09.002

Kokubo, T., and Takadama, H. (2006). How Useful Is SBF in Predicting *In Vivo* Bone Bioactivity? *Biomaterials* 27 (15), 2907–2915. doi:10.1016/j.biomaterials.2006.01.017

Lala, S., Satpati, B., and Pradhan, S. K. (2016). Sintering Behavior and Growth Mechanism of β-TCP in Nanocrystalline Hydroxyapatite Synthesized by Mechanical Alloying. *Ceramics Int.* 42 (11), 13176–13182. doi:10.1016/j.ceramint.2016.05.109

Liang, L., and Ruckenstein, E. (1996). Pervaporation of Ethanol-Water Mixtures through Polydimethylsiloxane-Polystyrene Interpenetrating Polymer Network Supported Membranes. *J. Membr. Sci.* 114 (2), 227–234. doi:10.1016/0376-7388(95)00319-3

Liang, J.-Z., Zhou, L., Tang, C.-Y., and Tsui, C.-P. (2013). Crystallization Properties of Polycaprolactone Composites Filled with Nanometer Calcium Carbonate. *J. Appl. Polym. Sci.* 128 (5), 2940–2944. doi:10.1002/app.38359

Loher, S., Reboul, V., Brunner, T. J., Simonet, M., Dora, C., Neuenschwander, P., et al. (2006). Improved Degradation and Bioactivity of Amorphous Aerosol Derived Tricalcium Phosphate Nanoparticles in Poly(lactide-Co-Glycolide). *Nanotechnology* 17 (8), 2054–2061. doi:10.1088/0957-4484/17/8/044

Luo, W., Charara, M., Saha, M. C., and Liu, Y. (2019). Fabrication and Characterization of Porous CNF/PDMS Nanocomposites for Sensing Applications. *Appl. Nanosci.* 9 (6), 1309–1317. doi:10.1007/s13204-019-00958-x

Ma, P. X., Zhang, R., Xiao, G., and Franceschi, R. (2001). Engineering New Bone Tissuein Vitro on Highly Porous Poly(?-Hydroxyl Acids)/hydroxyapatite Composite Scaffolds. *J. Biomed. Mater. Res.* 54 (2), 284–293. doi:10.1002/1097-4636(200102)54:2<284::aid-jbm16>3.0.co;2-w

Maeda, H., Maquet, V., Kasuga, T., Chen, Q. Z., Roether, J. A., and Boccaccini, A. R. (2007). Vaterite Deposition on Biodegradable Polymer Foam Scaffolds for Inducing Bone-like Hydroxycarbonate Apatite Coatings. *J. Mater. Sci. Mater. Med.* 18 (12), 2269–2273. doi:10.1007/s10856-007-3108-4

Miola, M., Verné, E., Ciraldo, F. E., Cordero-Arias, L., and Boccaccini, A. R. (2015). Electrophoretic Deposition of chitosan/45S5 Bioactive Glass Composite Coatings Doped with Zn and Sr. *Front. Bioeng. Biotechnol.* 3, 159. doi:10.3389/fbioe.2015.00159

Mohandes, F., and Salavati-Niasari, M. (2014a). *In Vitro* comparative Study of Pure Hydroxyapatite Nanorods and Novel Polyethylene Glycol/graphene Oxide/Hydroxyapatite Nanocomposite. *J. Nanopart. Res.* 16 (9), 1–12. doi:10.1007/s11051-014-2604-y

Mohandes, F., and Salavati-Niasari, M. (2014b). Freeze-Drying Synthesis, Characterization and *In Vitro* Bioactivity of Chitosan/graphene Oxide/hydroxyapatite Nanocomposite. *RSC Adv.* 4 (49), 25993–26001. doi:10.1039/C4RA03534H

Mondal, S., Nguyen, T. P., Pham, V. H., Hoang, G., Manivasagan, P., Kim, M. H., et al. (2020). Hydroxyapatite Nano Bioceramics Optimized 3D Printed Poly Lactic Acid Scaffold for Bone Tissue Engineering Application. *Ceramics Int.* 46 (3), 3443–3455. doi:10.1016/j.ceramint.2019.10.057

Nag, A., Afasrimanesh, N., Feng, S., and Mukhopadhyay, S. C. (2018a). Strain Induced Graphite/PDMS Sensors for Biomedical Applications. *Sensors Actuators A: Phys.* 271, 257–269. doi:10.1016/j.sna.2018.01.044

Nag, A., Feng, S., Mukhopadhyay, S. C., Kosel, J., and Inglis, D. (2018b). 3D Printed Mould-Based Graphite/PDMS Sensor for Low-Force Applications. *Sensors Actuators A: Phys.* 280, 525–534. doi:10.1016/j.sna.2018.08.028

Nagase, M., Chen, R.-B., Asada, Y., and Nakajima, T. (1989). Radiographic and Microscopic Evaluation of Subperiosteally Implanted Blocks of Hydrated and Hardened α-tricalcium Phosphate in Rabbits. *J. Oral Maxillofac. Surg.* 47 (6), 582–586. doi:10.1016/S0278-2391(89)80073-4

Ninago, M. D., Satti, A. J., Ciolino, A. E., and Villar, M. A. (2013). Influence of Amorphous Block on the thermal Behavior of Well-Defined Block Copolymers Based on ε-caprolactone. *J. Therm. Anal. Calorim.* 112 (3), 1277–1287. doi:10.1007/s10973-012-2673-z

Ninago, M. D., López, O. V., Lencina, M. M. S., García, M. A., Andreucetti, N. A., Ciolino, A. E., et al. (2015). Enhancement of Thermoplastic Starch Final Properties by Blending with Poly(ε-Caprolactone). *Carbohydr. Polym.* 134, 205–212. doi:10.1016/j.carbpol.2015.08.007

Ninago, M. D., Hanazumi, V., Passaretti, M. G., Vega, D. A., Ciolino, A. E., and Villar, M. A. (2017). Enhancement of Mechanical and Optical Performance of Commercial Polystyrenes by Blending with Siloxane-Based Copolymers. *J. Appl. Polym. Sci.* 134 (30), 45122. doi:10.1002/app.45122

Ninago, M. D., Ciolino, A. E., and Villar, M. A. (2020). Improvement in Poly(ε-Caprolactone) Bio-Activity. Structural Characterization and *In Vitro* Assessment. *Int. J. Polymeric Mater. Polymeric Biomater.* 69 (4), 201–210. doi:10.1080/00914037.2018.1552864

Öztürk, T., and Meyvacı, E. (2017). Synthesis and Characterization Poly(ε-Caprolactone-B-Ethylene Glycol-B-ε-Caprolactone) ABA Type Block Copolymers via "Click" Chemistry and Ring-Opening Polymerization. *J. Macromol. Sci. A* 54 (9), 575–581. doi:10.1080/10601325.2017.1309251

Öztürk, T., Atalar, M. N., Göktaş, M., and Hazer, B. (2013). One-step Synthesis of Block-Graft Copolymers via Simultaneous Reversible-Addition Fragmentation Chain Transfer and Ring-Opening Polymerization Using a Novel Macroinitiator. *J. Polym. Sci. Part. A: Polym. Chem.* 51 (12), 2651–2659. doi:10.1002/pola.26654

Öztürk, T., Yavuz, M., Göktaş, M., and Hazer, B. (2016). One-step Synthesis of Triarm Block Copolymers by Simultaneous Atom Transfer Radical and Ring-

Opening Polymerization. *Polym. Bull.* 73 (6), 1497–1513. doi:10.1007/s00289-015-1558-2

Park, C.-H., Kim, E. K., Tijing, L. D., Amarjargal, A., Pant, H. R., Kim, C. S., et al. (2014). Preparation and Characterization of LA/PCL Composite Fibers Containing Beta Tricalcium Phosphate (β-TCP) Particles. *Ceramics Int.* 40 (3), 5049–5054. doi:10.1016/j.ceramint.2013.10.016

Peña, J., and Vallet-Regı, M. (2003). Hydroxyapatite, Tricalcium Phosphate and Biphasic Materials Prepared by a Liquid Mix Technique. *J. Eur. Ceram. Soc.* 23 (10), 1687–1696. doi:10.1016/S0955-2219(02)00369-2

Pereira, H. F., Cengiz, I. F., Silva, F. S., Reis, R. L., and Oliveira, J. M. (2020). Scaffolds and Coatings for Bone Regeneration. *J. Mater. Sci. Mater. Med.* 31 (3), 1–16. doi:10.1007/s10856-020-06364-y

Persenaire, O., Alexandre, M., Degée, P., and Dubois, P. (2001). Mechanisms and Kinetics of Thermal Degradation of Poly(ε-Caprolactone). *Biomacromolecules* 2 (1), 288–294. doi:10.1021/bm0056310

Pishbin, F., Cordero-Arias, L., Cabanas-Polo, S., and Boccaccini, A. R. (2015). "Bioactive Polymer-Calcium Phosphate Composite Coatings by Electrophoretic Deposition," in *Surface Coating and Modification of Metallic Biomaterials* (United Kingdom: Woodhead Publishing), 359–377. doi:10.1016/B978-1-78242-303-4.00012-0

Qu, H., Fu, H., Han, Z., and Sun, Y. (2019). Biomaterials for Bone Tissue Engineering Scaffolds: A Review. *RSC Adv.* 9 (45), 26252–26262. doi:10.1039/C9RA05214C

Quiroga, G. A. R., Redondo, F. L., Ninago, M. D., Ciolino, A. E., Villar, M. A., and Santillán, M. J. (2018). Fabricación de Recubrimientos compuestos de Bioglass®/poli (ε-caprolactona) Obtenidos por Co-Deposición Electroforética Sobre Acero Inoxidable. *Matéria (Rio de Janeiro)* 23 (02), 1–12. doi:10.1590/s1517-707620180002.0431

Raj, A., Suthanthiraraj, P. P. A., and Sen, A. K. (2018). Pressure-Driven Flow through PDMS-Based Flexible Microchannels and Their Applications in Microfluidics. *Microfluid Nanofluid* 22 (11), 1–25. doi:10.1007/s10404-018-2150-5

Ramezani, S., Emadi, R., Kharaziha, M., and Tavangarian, F. (2017). Synthesis, Characterization and *In Vitro* Behavior of Nanostructured Diopside/biphasic Calcium Phosphate Scaffolds. *Mater. Chem. Phys.* 186, 415–425. doi:10.1016/j.matchemphys.2016.11.013

Raynaud, S., Champion, E., Bernache-Assollant, D., and Thomas, P. (2002). Calcium Phosphate Apatites with Variable Ca/P Atomic Ratio I. Synthesis, Characterisation and thermal Stability of Powders. *Biomaterials* 23 (4), 1065–1072. doi:10.1016/S0142-9612(01)00218-6

Redondo, F. L., Ninago, M. D., de Freitas, A. G. O., Giacomelli, C., Ciolino, A. E., and Villar, M. A. (2018). Tailor-Made, Linear, and "Comb-Like" Polyester-Based Copolymers: Synthesis, Characterization, and Thermal Behavior of Potential 3D-Printing/Electrospinning Candidates. *Int. J. Polym. Sci.* 2018, 1–15. doi:10.1155/2018/8252481

Redondo, F. L., Quiroga, G. A. R., de Freitas, A. G. O., Villar, M. A., Ninago, M. D., and Ciolino, A. E. (2020). Composite Coatings Based on Linear and Branched Block Copolymers for Hydroxyapatite Deposition in Simulated Body-Fluid. *Polymer-Plastics Tech. Mater.* 59 (9), 985–997. doi:10.1080/25740881.2020.1719138

Redondo, F. L. (2018). *Síntesis y caracterización de copolímeros bloque biocompatibles. Thesis, Bahía Blanca*. Argentina: Universidad Nacional del Sur. Available at: http://repositoriodigital.uns.edu.ar/handle/123456789/4168.

Reid, J. W., Tuck, L., Sayer, M., Fargo, K., and Hendry, J. A. (2006). Synthesis and Characterization of Single-phase Silicon-Substituted α-tricalcium Phosphate. *Biomaterials* 27 (15), 2916–2925. doi:10.1016/j.biomaterials.2006.01.007

Roether, J. A., Boccaccini, A. R., Hench, L. L., Maquet, V., Gautier, S., and Jérôme, R. (2002). Development and *In Vitro* Characterisation of Novel Bioresorbable and Bioactive Composite Materials Based on Polylactide Foams and Bioglass for Tissue Engineering Applications. *Biomaterials* 23 (18), 3871–3878. doi:10.1016/S0142-9612(02)00131-X

Sartore, L., Inverardi, N., Pandini, S., Bignotti, F., and Chiellini, F. (2019). PLA/PCL-based Foams as Scaffolds for Tissue Engineering Applications. *Mater. Today Proc.* 7, 410–417. doi:10.1016/j.matpr.2018.11.103

Satti, A. J., de Freitas, A. G. O., Marani, M. L. S., Villar, M. A., Vallés, E. M., Giacomelli, C., et al. (2017). Anionic Ring Opening Polymerization of ε-Caprolactone Initiated by Lithium Silanolates. *Aust. J. Chem.* 70 (1), 106–112. doi:10.1071/CH16270

Savaş, B., Çatıker, E., Öztürk, T., and Meyvacı, E. (2021). Synthesis and Characterization of Poly(α-Methyl β-alanine)-poly(ε-caprolactone) Tri Arm star Polymer by Hydrogen Transfer Polymerization, Ring-Opening Polymerization and "click" Chemistry. *J. Polym. Res.* 28 (2), 1–10. doi:10.1007/s10965-020-02367-z

Seuss, S., Heinloth, M., and Boccaccini, A. R. (2016). Development of Bioactive Composite Coatings Based on Combination of PEEK, Bioactive Glass and Ag Nanoparticles with Antibacterial Properties. *Surf. Coat. Tech.* 301, 100–105. doi:10.1016/j.surfcoat.2016.03.057

Shah Mohammadi, M., Rezabeigi, E., Bertram, J., Marelli, B., Gendron, R., Nazhat, S. N., et al. (2020). Poly(d,l-Lactic Acid) Composite Foams Containing Phosphate Glass Particles Produced via Solid-State Foaming Using CO2 for Bone Tissue Engineering Applications. *Polymers* 12 (1), 231. doi:10.3390/polym12010231

Somrani, S., Rey, C., and Jemal, M. (2003). Thermal Evolution of Amorphous Tricalcium Phosphate. *J. Mater. Chem.* 13 (4), 888–892. doi:10.1039/B210900J

Suchanek, W., and Yoshimura, M. (1998). Processing and Properties of Hydroxyapatite-Based Biomaterials for Use as Hard Tissue Replacement Implants. *J. Mater. Res.* 13 (1), 94–117. doi:10.1557/JMR.1998.0015

Sultana, N. (2018). "Mechanical and Biological Properties of Scaffold Materials," in *Functional 3D Tissue Engineering Scaffolds* (United Kingdom: Woodhead Publishing), 1–21. doi:10.1016/B978-0-08-100979-6.00001-X

Sungsee, P., and Tanrattanakul, V. (2019). Biocomposite Foams from Poly(lactic Acid) and Rubber wood Sawdust: Mechanical Properties, Cytotoxicity, and *In Vitro* Degradation. *J. Appl. Polym. Sci.* 136 (48), 48259. doi:10.1002/app.48259

Taale, M., Krüger, D., Ossei-Wusu, E., Schütt, F., Rehman, M. A. U., Mishra, Y. K., et al. (2019). Systematically Designed Periodic Electrophoretic Deposition for Decorating 3D Carbon-Based Scaffolds with Bioactive Nanoparticles. *ACS Biomater. Sci. Eng.* 5 (9), 4393–4404. doi:10.1021/acsbiomaterials.9b00102

Thinakaran, S., Loordhuswamy, A., and Venkateshwapuram Rengaswami, G. (2020). Electrophoretic Deposition of Chitosan/nano Silver Embedded Micro Sphere on Centrifugal Spun Fibrous Matrices - A Facile Biofilm Resistant Biocompatible Material. *Int. J. Biol. Macromol.* 148, 68–78. doi:10.1016/j.ijbiomac.2020.01.086

Uhrig, D., and Mays, J. W. (2005). Experimental Techniques in High-Vacuum Anionic Polymerization. *J. Polym. Sci. A. Polym. Chem.* 43 (24), 6179–6222. doi:10.1002/pola.21016

Wang, C., Ma, J., Cheng, W., and Zhang, R. (2002). Thick Hydroxyapatite Coatings by Electrophoretic Deposition. *Mater. Lett.* 57 (1), 99–105. doi:10.1016/S0167-577X(02)00706-1

Wang, L., Wang, D., Zhou, Y., Zhang, Y., Li, Q., and Shen, C. (2019). Fabrication of Open-porous PCL/PLA Tissue Engineering Scaffolds and the Relationship of Foaming Process, Morphology, and Mechanical Behavior. *Polym. Adv. Technol.* 30 (10), 2539–2548. doi:10.1002/pat.4701

Wietor, J.-L., Van Beek, D. J. M., Peters, G. W., Mendes, E., and Sijbesma, R. P. (2011). Effects of Branching and Crystallization on Rheology of Polycaprolactone Supramolecular Polymers with Ureidopyrimidinone End Groups. *Macromolecules* 44 (5), 1211–1219. doi:10.1021/ma1026065

Wolf, M. P., Salieb-Beugelaar, G. B., and Hunziker, P. (2018). PDMS with Designer Functionalities-Properties, Modifications Strategies, and Applications. *Prog. Polym. Sci.* 83, 97–134. doi:10.1016/j.progpolymsci.2018.06.001

Wu, N., Huang, L., and Zheng, A. (2006). Synthesis and Properties of Polystyrene/polydimethylsiloxane Graft Copolymers. *Front. Chem. China* 1 (3), 350–356. doi:10.1007/s11458-006-0043-4

Yam, W. Y., Ismail, J., Kammer, H. W., Schmidt, H., and Kummerlöwe, C. (1999). Polymer Blends of Poly(ε-Caprolactone) and Poly(vinyl Methyl Ether) - Thermal Properties and Morphology. *Polymer* 40 (20), 5545–5552. doi:10.1016/S0032-3861(98)00807-6

Yang, C. R., Wang, Y. J., Chen, X. F., and Zhao, N. R. (2005). Biomimetic Fabrication of BCP/COL/HCA Scaffolds for Bone Tissue Engineering. *Mater. Lett.* 59 (28), 3635–3640. doi:10.1016/j.matlet.2005.07.022

Yang, Y., Michalczyk, C., Singer, F., Virtanen, S., and Boccaccini, A. R. (2015). *In Vitro* study of Polycaprolactone/bioactive Glass Composite Coatings on Corrosion and Bioactivity of Pure Mg. *Appl. Surf. Sci.* 355, 832–841. doi:10.1016/j.apsusc.2015.07.053

Yazdimamaghani, M., Razavi, M., Vashaee, D., Pothineni, V. R., Rajadas, J., and Tayebi, L. (2015). Significant Degradability Enhancement in Multilayer Coating

of Polycaprolactone-Bioactive Glass/gelatin-Bioactive Glass on Magnesium Scaffold for Tissue Engineering Applications. *Appl. Surf. Sci.* 338, 137–145. doi:10.1016/j.apsusc.2015.02.120

Yeong, W. Y., Sudarmadji, N., Yu, H. Y., Chua, C. K., Leong, K. F., Venkatraman, S. S., et al. (2010). Porous Polycaprolactone Scaffold for Cardiac Tissue Engineering Fabricated by Selective Laser Sintering. *Acta Biomater.* 6 (6), 2028–2034. doi:10.1016/j.actbio.2009.12.033

Yu, Y., Mathew, R., and Edén, M. (2018). Quantitative Composition-Bioactivity Relationships of Phosphosilicate Glasses: Bearings from the Phosphorus Content and Network Polymerization. *J. Non-Cryst. Sol.* 502, 106–117. doi:10.1016/j.jnoncrysol.2018.07.060

Zhang, K., Wang, Y., Hillmyer, M. A., and Francis, L. F. (2004). Processing and Properties of Porous Poly(l-Lactide)/bioactive Glass Composites. *Biomaterials* 25 (13), 2489–2500. doi:10.1016/j.biomaterials.2003.09.033

Zhao, J., Guo, L. Y., Yang, X. B., and Weng, J. (2008). Preparation of Bioactive Porous HA/PCL Composite Scaffolds. *Appl. Surf. Sci.* 255 (5), 2942–2946. doi:10.1016/j.apsusc.2008.08.056

Zhao, N., Lv, Z., Ma, J., Zhu, C., and Li, Q. (2019). Fabrication of Hydrophilic Small Diameter Vascular Foam Scaffolds of Poly(ε-Caprolactone)/Polylactic Blend by Sodium Hydroxide Solution. *Eur. Polym. J.* 110, 31–40. doi:10.1016/j.eurpolymj.2018.11.011

Zhou, H., and Lee, J. (2011). Nanoscale Hydroxyapatite Particles for Bone Tissue Engineering. *Acta Biomater.* 7 (7), 2769–2781. doi:10.1016/j.actbio.2011.03.019

Conflict of Interest: The authors declare that the research was conducted in the absence of any commercial or financial relationships that could be construed as a potential conflict of interest.

Publisher's Note: All claims expressed in this article are solely those of the authors and do not necessarily represent those of their affiliated organizations, or those of the publisher, the editors, and the reviewers. Any product that may be evaluated in this article, or claim that may be made by its manufacturer, is not guaranteed or endorsed by the publisher.